Applied Catalysis B: Environmental 132–133 (2013) 170–182

Contents lists available at SciVerse ScienceDirect

Applied Catalysis B: Environmental

journal homepage: www.elsevier.com/locate/apcatb

Glycerol conversion to acrylonitrile by consecutive dehydration over WO_3/TiO_2 and ammoxidation over Sb-(Fe,V)-O

Carsten Liebig[a,b,c], Sébastien Paul[a,c,d,*], Benjamin Katryniok[a,c,d], Cyrille Guillon[a,c], Jean-Luc Couturier[e], Jean-Luc Dubois[e], Franck Dumeignil[a,c,f], Wolfgang F. Hoelderich[b]

[a] Univ. Lille Nord de France, F-59000, Lille, France
[b] Department of Chemical Technology and Heterogeneous Catalysis, RWTH Aachen University, Worringerweg 1, D-52074 Aachen, Germany
[c] Unité de Catalyse et de Chimie du Solide, UCCS (UMR CNRS 8181), Cité Scientifique, F-59650, Villeneuve d'Ascq, France
[d] Ecole Centrale de Lille, ECLille, F-59655, Villeneuve d'Ascq, France
[e] ARKEMA, Centre de Recherche Rhône Alpes, Pierre Bénite, F-69493, France
[f] Institut Universitaire de France, Maison des Universités, 103 Boulevard Saint-Michel, 75005 Paris, France

ARTICLE INFO

Article history:
Received 7 July 2012
Received in revised form 1 November 2012
Accepted 23 November 2012
Available online 30 November 2012

Keywords:
Glycerol
Indirect ammoxidation
Acrolein
Acrylonitrile
Tandem-reactor

ABSTRACT

The indirect ammoxidation of glycerol to acrylonitrile *via* intermediate formation of acrolein was studied using a tandem reactor coupling a dehydration step with an ammoxidation step. For the first step of dehydration of glycerol to acrolein, we used a previously optimized WO_3/TiO_2 catalyst, while Sb-V-O or Sb-Fe-O catalysts were developed and used for the subsequent ammoxidation step. Especially, the Sb-Fe-O catalysts were found highly selective and thus were more-deeply investigated. The corresponding catalysts were characterized by nitrogen physisorption, X-ray powder diffraction, thermogravimetric analysis, X-ray photoelectron spectroscopy, and temperature-programmed reduction in the presence of H_2. We found that the presence of a $FeSbO_4$ mixed phase on the synthesized samples was correlated to a high selectivity to acrylonitrile. Further, we observed an increase in selectivity to acrylonitrile with the reaction time, which was explained by the progressive formation of additional amounts of $FeSbO_4$ on the catalysts during the reaction. Finally, the reaction parameters (temperature, catalyst amount, molar NH_3/AC ratio and molar O_2/AC ratio) for the catalyst with an Sb/Fe molar ratio of 0.6 were optimized, whereby a maximum yield in acrylonitrile of 40% (based on glycerol) could be achieved.

1. Introduction

The finiteness of fossil feedstock for fuels and the increasing number of the global vehicle fleet from approximately 1 billion nowadays (commercial vehicles and passenger cars) to 1.6 billion by 2030 urge the need for the development of renewables-based fuels such as, for instance, biodiesel obtained by transesterification of fats or oils [1,2]. The European Union has defined that, by 2020, all the domestic transportation fuels (gasoline and diesel) sold in the EU must be blended with about 10% of bio-fuel [3]. In order to achieve such requirements, the production of biodiesel has drastically increased during the last decade [4]. Consequently, the availability of glycerol has increased as well, since approximately 10 wt.% of glycerol are by-produced during the biodiesel process. Estimations indicate that the supply of glycerol will overpass the actual demand by at least six times in 2020 [5]. Due to this oversupply, glycerol has become a very interesting starting material for the chemical industry [6–10]. One well known upgrading technology for glycerol is its dehydration to acrolein (AC), which has been the object of extensive research efforts during the last decade [11–25]. Acrolein is industrially used to produce methionine and acrylic acid, but has also several other minor applications [26]. In fact, acrolein is also considered as potentially being an interesting intermediate for the production of acrylonitrile (ACN) *via* ammoxidation over redox catalysts, but this technology is not yet mature for commercialization at the industrial scale [27–29]. ACN is used as a raw material for producing acrylic fibers, ABS (acrylonitrile-butadiene-styrene) and SAN (styrene-acrylonitrile) resins. It is also an intermediate in the production process of adiponitrile and acrylamide [30].

Nowadays, ACN is almost exclusively produced by the SOHIO process, which was developed by the Standard Oil of Ohio company during the fifties of the last century. In this process, propene is directly converted to ACN in the presence of air and ammonia over the so-called multicomponent catalysts (MCC) based on bismuth-molybdenum oxides with yields higher than 70% [30,31]. Alternative processes use, for example, propane as a feedstock, but

* Corresponding author at: Ecole Centrale de Lille, Cité Scientifique BP48, F-59650, Villeneuve d'Ascq, France. Tel.: +33 0320335457.
E-mail address: sebastien.paul@ec-lille.fr (S. Paul).

0926-3373/$ – see front matter © 2012 Elsevier B.V. All rights reserved.
http://dx.doi.org/10.1016/j.apcatb.2012.11.035

the yield is then lower compared to the propene-based process (60% compared to yields higher than 70% for propene) [30,32]. Nevertheless, as the availability of propene is limited due to its fossil origin, the development of a sustainable alternative pathway from renewables is of topical interest. In fact, a process combining the dehydration of glycerol to acrolein with the ammoxidation of the latter to acrylonitrile would be an alternative to the production processes based on fossil feedstocks. The realization of the two reactions can be either envisioned using one single multi-functional catalyst, which promotes both reactions (direct route), or with two different catalysts – separately optimized for each reaction step – (indirect route) and sequentially working in two coupled reactors.

The direct ammoxidation of glycerol to acrylonitrile has indeed been described in the literature. However, only very few papers are available on this particular reaction. Bañares et al. showed that the direct conversion of glycerol to acrylonitrile is possible over mixed oxides containing Sb, V and Nb. They report a maximum yield in ACN of 48% [33,34]. We tried several times to reproduce the results published by Bañares et al., but the experiments resulted always in full conversion of glycerol with the formation of only traces of the desired product ACN (2% of selectivity in a typical experiment) with the main product being CO_2 (50% in yield). Therefore, the indirect route is supposedly more promising as it allows the independent choice of the catalyst and the reaction conditions. Furthermore, one has to keep in mind the compatibility of the catalyst and the conditions: For example, the catalyst for the first reaction step (dehydration) generally exhibits acidity, which may cause problems considering the presence of NH_3 in the feed. This latter will most probably block the acidic centers of the catalyst used for dehydration. Additionally, the ammoxidation of acrolein is usually carried out at elevated reaction temperature compared to the dehydration of glycerol (step I: 270–300 °C *vs.* step II: 400–500 °C).

Thus, we focused our investigations on the indirect route. The first step, *i.e.*, the catalytic dehydration of glycerol in the gaseous phase using acid catalysts is well described in the literature [15,35,36]. According to previous results of Hoelderich's group, the WO_3/TiO_2 system proved to be very efficient for the dehydration of glycerol to AC, with yields above 70% and limited side-products formation (acetaldehyde, hydroxyacetone, acetic acid) [15]. In contrast, the second step of ammoxidation of acrolein has been scarcely discussed in the literature [27–29,37,38]. Furthermore, when considering a tandem approach *via* intermediate formation of AC, the feed of the second reaction step contains impurities (aforementioned side-products) from the first step of dehydration of glycerol – including large amounts of water –, which impose the use of ammoxidation catalysts with an increased tolerance, especially towards water, but also of which the performances are not altered by the presence of organic impurities. Mixed oxides based on antimony/iron and antimony/vanadium are known to work for ammoxidation of AC in the presence of water. For instance, Germain et al. studied the acrolein ammoxidation over a Sn-Sb-Fe-O catalyst in the presence of water [39]. Even though the steam did not improve the yield in ACN, the conversion rate of AC was found six times faster than in the case of propene ammoxidation. Nilsson et al. found that the addition of steam to the feed can even increase the reaction rate and the selectivity to ACN over Sb-V-O catalysts originally developed for the ammoxidation of propane [40].

Therefore, the objective of the present work was to study the indirect ammoxidation of glycerol to ACN, *via* AC as an intermediate, in a continuous gas flow reactor running in the tandem mode over WO_3/TiO_2 (dehydration step) and SbV-O or Sb-Fe-O (ammoxidation step) catalysts. The main focus was put on the study of the ammoxidation step under feed conditions simulating the expected acrolein/water ratio obtained by dehydration of glycerol to AC over previously developed and well known WO_3/TiO_2 catalysts [15]. The catalytic performances of Sb-Fe-O and Sb-V-O catalysts were evaluated and optimized by tuning the reaction temperature, the molar NH_3/AC ratio, the molar O_2/AC ratio and the amount of catalyst. In addition, the feasibility of the indirect ammoxidation of glycerol to ACN in a tandem-reaction was demonstrated (proof of concept).

2. Experimental

2.1. Catalyst and reactants

The catalyst used for the dehydration of glycerol was prepared according to the slurry method described by Ulgen et al. [15]. The WO_3 loading was 13.2 wt.%. The TiO_2 support (Hombikat Typ II) was kindly provided by Sachtleben AG, Germany.

Several antimony iron mixed oxide catalysts were prepared according to the deposition method described by Li et al. [41].

An appropriate amount of iron nitrate, $Fe(NO_3)_3{\cdot}9H_2O$ (Merck) was dissolved in 500 mL of an aqueous oxalic acid solution (0.1 N; Aldrich). Thereafter, the solution was heated to 80 °C and the appropriate amount of antimony-III-oxide (Sb_2O_3; Alfa Aesar) was added under stirring. The resulting solution temperature was maintained between 80 and 90 °C under stirring for 3 h in order to evaporate the solvent. Afterwards, the resulting cake was dried at 100 °C for 72 h. The catalyst powder was then pressed to pellets before being crushed and sieved to obtain a particle size between 0.5 and 1 mm. Finally, the catalyst particles were calcined at 500 °C under air for 8 h.

The antimony vanadium mixed oxide was prepared following the method described by Nilsson et al. [40].

Ammonium metavanadate NH_4VO_3 (ABCR GmbH) was dissolved in hot water (80 °C). After addition of antimony-III-oxide (Sb_2O_3; Alfa Aesar), the solution was heated under reflux with stirring over night. Thereafter, the excess water was evaporated at a temperature between 80 and 90 °C. The remaining cake was dried at 110 °C overnight and afterwards at 350 °C under air. Thereupon, the catalyst powder was pressed to pellets before being crushed and sieved to obtain a particle size of 0.5 to 1 mm. At last, the particles were calcined at 610 °C in air.

The catalysts were named according to their composition and theoretical molar ratio of the single components. For example, the antimony iron mixed oxide with a molar Sb/Fe ratio of 0.8 was named SbFeO0.8, whereas the antimony vanadium mixed oxide with the same molar ratio was be named SbVO0.8.

Glycerol (Aldrich, 99%) and acrolein (Fluka, 95%) were used to prepare the feed solutions for the dehydration and the ammoxidation reactions, respectively. High purity oxygen (Westfalen or Air-Liquide, 99.9%) and ammonia (Westfalen, 99.9%) were purchased.

2.2. Ammoxidation catalyst characterization

The specific surface areas (S_{BET}) and total pore volumes (V_p) were measured by the N_2 physisorption/desorption technique, using a Micromeritics ASAP 2010 analyser at the liquid nitrogen temperature (77 K). The specific surface areas were calculated using the BET (Brunauer–Emmett–Teller) method. The total pore volume was determined using the point measured at a relative pressure P/P_0 of 0.995. The samples were outgassed at 150 °C for 3 h prior to analysis.

Thermogravimetry (TG) analyses were performed using a TA instruments (Model 2960 SDT, V3.0F) to study the thermal decomposition behaviour of the fresh (meaning calcined but not used in a catalytic test) and spent (meaning calcined and used in a catalytic

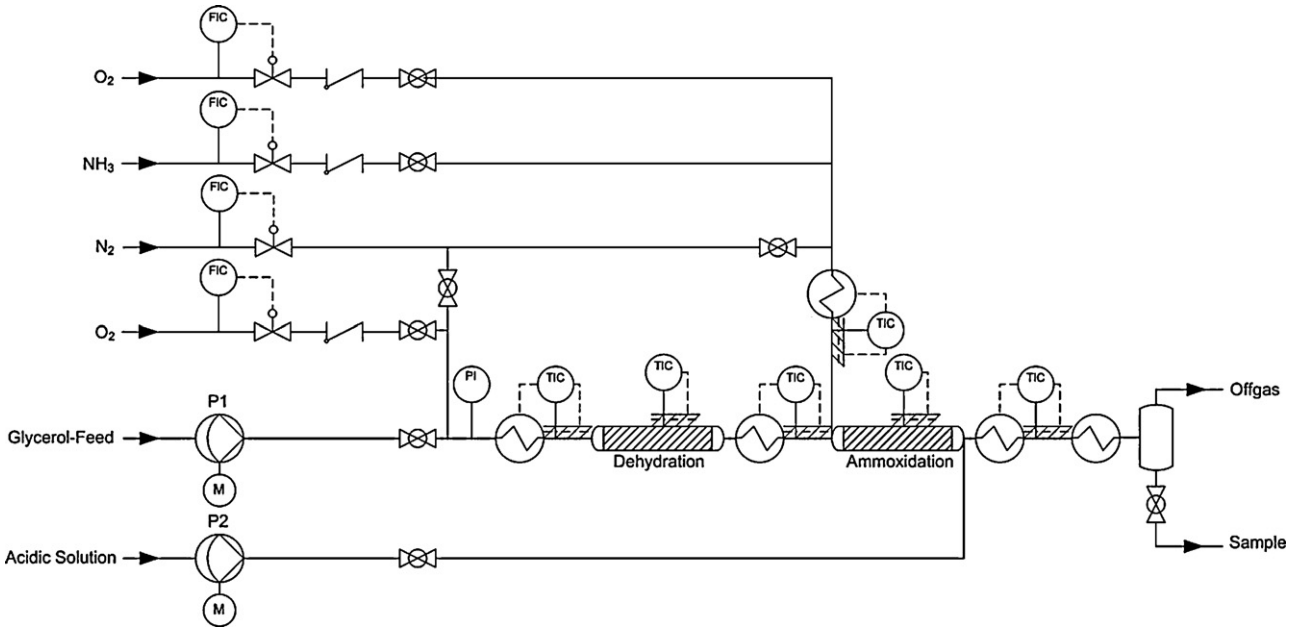

Fig. 1. Schematics of the reactor setup for the tandem process.

test) catalysts. The catalysts were heated from room temperature to 700 °C with an increasing rate of 3 °C/min under air flow.

The crystalline structures of the catalysts were determined by the X-ray diffraction (XRD) technique on a Bruker D8 Advance diffractometer, using the CuKα radiation (λ = 1.5506 Å) as an X-ray source. A range from 5° < 2θ <80° was scanned by steps of 0.05°/s and with an 1 s acquisition time.

X-ray photoelectron spectroscopy (XPS) surface analyses were carried out using a Kratos Axis Ultra DLD apparatus equipped with a hemispherical analyser and a delay line detector. The spectra were recorded using an Al mono-chromated X-ray source (10 kV, 15 mA) with a pass energy of 40 eV (0.1 eV/step) for high resolution spectra, and a pass energy of 160 eV (1 eV/step), for the survey spectrum in hybrid mode and slot lens mode, respectively.

The reducibility of the catalysts was evaluated by temperature-programmed reduction (TPR) at atmospheric pressure. 100 mg of sample were loaded into a quartz reactor and pre-treated by a He flow (30 mL/min) at 100 °C for 2 h. Then, the pure helium flow was replaced by the reductive gas H_2/He (5 mol.% H_2 in He) at a flow-rate of 30 mL/min. The temperature of the reactor was linearly increased from 100 to 800 °C at a rate of 5 °C/min. The effluent gas was analysed by a thermal conductivity detector (TCD).

2.3. Experimental setup for the evaluation of the catalytic performances

A schematic diagram of the integrated setup used for the indirect ammoxidation of glycerol is shown in Fig. 1. The setups used for the decoupled dehydration of glycerol and the ammoxidation of acrolein were designed similarly.

All the reactions were performed under atmospheric pressure in continuous plug flow fixed-bed reactors designed under the form of a coil made of stainless steel with an inner diameter of 6 mm. Each reactor was placed in an electrically heated oven equipped with an air circulation system in order to maintain an uniform temperature distribution in the oven. All the reactors were connected to an evaporator that was used to ensure vaporisation of the liquid reactants before contacting the catalytic bed. It was made of a stainless steel tube of an appropriate length, which was heated by a heating tape. The reactors were filled with granulated catalysts with a particle size of 0.5–1 mm. The reaction products were collected in a double-jacket separating funnel connected to a reflux condenser. The temperature of the cooling trap was maintained at -5 °C using a cryostat. In the case of the setup used for the ammoxidation of acrolein and of the setup used for the indirect ammoxidation of glycerol, the products were condensed in an acidic solution (5 wt.% acetic acid in water, 35 g in total) in order to immediately neutralize non-reacted ammonia in order to suppress ammonia-induced polymerization of acrolein. Additionally, an acidic solution (17 wt.% acetic acid in water, flow rate 17 g/h) was injected directly after the catalytic bed with the purpose of inhibiting the polymerization in the tubing between the reactor and the cooling trap. All the liquid reactants were pumped with diaphragm pumps (FINK). The flow rate of the gaseous reactants was controlled with mass-flow controllers (Brooks).

For the dehydration of glycerol, the parameters were fixed as the optimal ones found in our previous study [15]: the reaction temperature was set at 280 °C. 5 g of 13.2 wt.% or 15 wt.% WO_3/TiO_2 were used as the catalyst. The flow rate of the 20 wt.% aqueous glycerol solution was set to 23 g/h. The O_2 flow was adjusted to 11.33 mL/min at standard temperature and pressure. This quantity of oxygen was selected to suppress catalyst deactivation while avoiding the formation of oxidized by-products, as stated by Ulgen et al. [15].

The screening of the SbFeO and SbVO catalysts for the ammoxidation of acrolein was carried out at 400 °C. The molar NH_3/AC and O_2/AC ratios were set at 1.0 and 0.5, respectively. For each test, 5 g of catalyst were loaded into the reactor. An aqueous solution of acrolein (7.1 wt.%) was fed to the reactor at a flow rate of 48 g/h. These figures simulated a realistic yield of 62% in acrolein expected from the first reaction step (dehydration). The feed solution for the AC ammoxidation experiments was prepared by mixing the appropriate amount of synthetic acrolein with water.

The experimental design was generated by the statistical software Design-Expert, Version 5.0.8, Stat-Ease Inc. The response surface methodology was used in order to investigate the influence of the varied parameters (reaction temperature, catalyst amount, molar O_2/AC ratio, molar NH_3/AC ratio) on the response variables.

The parameters applied for the tandem reaction are described in Section 3.1.2.

2.4. Products analysis

The quantification of the liquid product samples was carried out using high-performance liquid chromatography (HPLC) and gas chromatography (GC). The samples were analysed by means of high-performance liquid chromatography on a Merck Hitachi apparatus, equipped with a refractive index detector and a Nucleogel Sugar 810 H column (length: 300 mm; inner diameter: 7.8 mm) maintained at 35 °C. The mobile phase was a 5 mM sulfuric acid solution pumped at 0.8 mL/min.

The gas chromatography measurements were performed on a CE Instruments GC 8000 TOP apparatus equipped with a flame ionization detector (FID) and an Alltech EC-1000 semi-capillary column (length: 30 m; diameter: 0.53 mm; film thickness: 1.2 μm) using helium as a carrier gas (Air Liquide, 99.999%). The temperature program used was: 40 °C for 7 min before heating to 240 °C with a ramp of 20 °C/min and hold 240 °C for 1 minute. The injector and detector temperatures were set at 240 °C.

The glycerol and AC conversions were calculated using the following Eq. (1):

$$X = \frac{n_{\text{Reactant,in}} - n_{\text{Reactant,out}}}{n_{\text{Reactant,in}}} \quad (1)$$

where n is the amount of the reactant (either glycerol or acrolein) in moles before and after reaction.

The selectivity to AC and ACN were calculated as depicted in Eq. (2) below, where n_{Product} is related either to acrolein or acrylonitrile.

$$S = \frac{n_{\text{Product}}}{n_{\text{Reactant,in}} - n_{\text{Reactant,out}}} \quad (2)$$

Due to technical limitations, analysis of the gaseous products as well as identification of by-products was only possible for some specific experiments. We verified that the main by-products for the indirect ammoxidation of glycerol to acrylonitrile are CO_2 (selectivity usually around 15%), acetaldehyde (selectivity usually of *ca.* 1%) and acetonitrile (selectivity usually of *ca.* 3%). Carbon monoxide could not be detected as it is normally formed in oxidation reactions in the presence of oxygen. A water gas shift reaction might happen forming CO_2 and H_2 out of CO. However, H_2 could not be detected due to experimental limitations. A typical carbon balance was 75% for those experiments. Therefore, we present the mass balance, even though the high water content might have some influence on the accuracy.

The mass balance of the experiments was calculated by dividing the weight of the liquid products condensed in the cooling trap by the sum of the reactants fed to the reactor.

3. Results and discussion

3.1. Catalytic performance tests

3.1.1. Preliminary tests – dehydration of glycerol

In a first approach, the dehydration of glycerol was studied using a WO_3/TiO_2 catalyst in a water-rich feed (80 wt.%). As aforementioned, the reaction conditions were chosen as those claimed as the optimal ones in the literature [15]. Table 1 shows that the glycerol conversion is stable during the first 3 h on stream. Afterwards, the conversion rate slightly decreases with time on stream (TOS). The selectivity towards AC reached 40% after 1 h and significantly increased within the next 2 h to 82%. Thereafter, the selectivity remained rather stable. In total, 96% conversion of glycerol and 70% selectivity towards AC were observed. The main by-products were hydroxyacetone (1.6%), acetaldehyde (1.5%) and propionaldehyde (2.0%). These results are in good agreement with those reported by Ulgen et al. [15].

Table 1
Catalytic performance of WO_3/TiO_2.

	1 h	2 h	3 h	4 h	5 h	Average
X glycerol, %	97	98	97	93	95	96
S acrolein, %	40	61	82	84	81	70
S hydroxyacetone, %	1.1	1.1	1.9	1.6	2.2	1.6
S acetaldehyde, %	1.7	1.9	1.3	1.5	1.2	1.5
S propionaldehyde, %	7.2	1.1	0.5	0.6	0.5	2.0

Reaction temperature: 280 °C; catalyst amount: 5.0 g; 11.33 mL/min O_2; contact time: 0.36 s; gas phase composition at 280 °C: 92.74% H_2O, 2.72% O_2, 4.54% glycerol.

The long-term stability of the WO_3/TiO_2 system was not investigated in this study as it was already studied by Ulgen et al. They showed that the glycerol conversion rate decreases exponentially from 100% to approximately 50% over 96 h of TOS [15].

These results illustrate that stable glycerol conversion with good yield in acrolein are obtained in this first reaction step. The efforts were then concentrated on the much more exploratory second step of acrolein ammoxidation.

3.1.2. Ammoxidation of acrolein

3.1.2.1. Preliminary catalytic tests with antimony-iron and antimony-vanadium mixed oxides. In a first series of experiments of AC ammoxidation, a SbFeO catalyst and a SbVO catalyst – both with a Sb/Fe and Sb/V ratio of 0.8 – were tested in order to compare their respective performances. The results are shown in Table 2. The AC conversion obtained over SbFeO0.8 was 80%. SbVO0.8 showed a somewhat lower conversion of 75%. The selectivity to acrylonitrile was considerably larger for SbFeO0.8 catalyst, exhibiting 31% after 5 h on stream, whereas in the case of SbVO0.8, the selectivity to ACN did not overpass 14%. Consequently, the yield in the desired product, *i.e.*, ACN reached 25% for the SbFeO catalyst and only 11% for the SbVO catalyst (Table 2).

The results obtained in the preliminary experiments thus encouraged us to focus on antimony-iron catalysts and to study the influence of their molar composition on their catalytic performances in the ammoxidation of acrolein.

3.1.2.2. Screening of antimony/iron ratio. Three additional SbFeO catalysts with molar Sb/Fe ratios of 0.4, 0.6 and 1.0 were subsequently tested. The results of the screening of their performances are given in Table 3, which gives the AC conversion as well as the ACN selectivity and the yield in ACN for each Sb/Fe ratio. In terms of acrolein conversion, no obvious trend can be noticed. The highest catalytic conversion of 80% was observed for the catalyst with

Table 2
Catalytic performance of SbFeO0.8 and SbVO0.8.

Catalyst	Molar ratio	Conversion, % AC	Selectivity, % ACN	Yield, % ACN	Mass balance, %
SbFeO	Sb/Fe 0.8	80	31	25	100.0
SbVO	Sb/V 0.8	75	14	11	97.9

Reaction temperature: 400 °C; catalyst amount: 5.0 g; reactants molar ratios: O_2/AC = 0.5 and NH_3/AC = 1.0; contact time: 0.12 s; gas phase composition at 400 °C: 94% H_2O, 1.2% O_2, 2.4% NH_3, 2.4% AC.

Table 3
Screening of Sb/Fe ratio: catalytic performances.

Catalyst	Conversion, %	Selectivity, %	Yield, %	Mass balance, %
	AC	ACN	ACN	
Sb/Fe 0.4	70	22	15	98.0
Sb/Fe 0.6	55	28	15	99.7
Sb/Fe 0.8	80	31	25	100.0
Sb/Fe 1.0	58	17	10	98.9

Reaction temperature 400 °C; catalyst amount 5.0 g; reactant ratio O_2/AC 0.5 and NH_3/AC 1.0; Contact time: 0.12 s; gas phase composition at 400 °C: 94% H_2O, 1.2% O_2, 2.4% NH_3, 2.4% AC.

a molar Sb/Fe ratio of 0.8. For the catalysts with molar ratios of 0.6 and 1.0, the catalytic activity was slightly lower, 55% and 58%, respectively. However, the catalytic conversion of the catalyst with a molar Sb/Fe ratio of 0.4 was 70%, namely the second best performance of the series. The yield in ACN was the same at 15% for SbFeO0.4 and SbFeO0.6. Afterwards, it reached a maximum with 25% for the catalyst with an Sb/Fe molar ratio of 0.8. In case of the catalyst with equimolar Sb/Fe ratio, the yield droped to its minimum of 10%. Thus, the SbFeO0.8 catalyst was clearly the best of the series in terms of catalytic performances and especially in terms of ACN yield.

Compared with results reported for the ammoxidation of acrolein in literature, the obtained yield in ACN over SbFeO0.8 is clearly lower. For example, the Distillers Company Limited filed a patent in 1959 dealing with the ammoxidation of acrolein over antimony tin mixed oxides, in which they reported a maximum yield of 74% [37]. However, in their case, the ammoxidation was carried out in the absence of water, thus indicating that water may possibly influence the catalytic performance in the ammoxidation of acrolein. Therefore, when comparing our results with those of the literature, one has to keep in mind that the feed to the second reaction step in the indirect ammoxidation of glycerol contains large amounts of water (approximately 87%).

3.1.2.3. Parameter optimization. As the results of the screening of the molar antimony to iron ratio were promising, a design of experiments (DoE) was carried out in order to optimize the key reaction parameters – reaction temperature, catalyst amount in order to vary the contact time, NH_3/AC molar ratio and O_2/AC molar ratio – for the catalyst with a molar Sb/Fe ratio of 0.6 as it exhibited medium values in terms of selectivity towards ACN (28%) and conversion of acrolein (54%), therefore, being suitable for studying the influence of the parameters on the ACN selectivity as well as the AC conversion. The SbFeO0.8 catalyst was not selected for the DoE as it already showed a high AC conversion and therefore, indicating less room for improvements in terms of catalytic activity compared to the SbFeO0.6 catalyst. The experimental design was generated by the statistical software Design Expert, Version 5.0.8, Stat-Ease Inc.

Fig. 2 illustrates the influence of the reaction temperature, the catalyst amount, and the O_2/AC and NH_3/AC ratios on the conversion of AC. Thereby, the conversion is increased with the amount of catalyst and the reaction temperature, reaching up to 82% for 6.5 g of catalyst at 425 °C. Furthermore, the conversion of AC also increased with the O_2/AC and NH_3/AC ratios. The highest acrolein conversion (88%) was obtained for an O_2/AC molar ratio of 5 and a NH_3/AC molar ratio of 1.5.

The influence of the parameters variations on the ACN selectivity is depicted in Fig. 3. At a reaction temperature of 375 °C and a relatively low catalyst mass of 3.5 g, the selectivity exhibited its overall minimum of 15%. In relation to the reaction temperature and the catalyst amount, the best selectivity of 30% was achieved at 400 °C over 5 g of catalyst. However, the selectivity showed a plateau at around 400 °C, whereby similar selectivity to ACN (around 30%) was achieved for catalyst amounts from 5.0 to 6.5 g.

The variation of the O_2/AC ratio resulted in an optimum for the selectivity to ACN at a molar ratio of 3.5, irrespective of the NH_3/AC ratio. This value is seven times higher than the stoichiometric ratio of oxygen. However, it is reported in the literature that O_2/AC molar ratios up to 10 can be applied [28]. No absolute optimum in terms of ACN selectivity was observed for the variation of the NH_3/AC ratio in the range between 0.5 and 1.5. The selectivity increased linearly with an increasing amount of NH_3 leading to the assumption that the selectivity to ACN can be still improved by applying higher NH_3/AC ratios. For further determination of the observed positive effect of higher NH_3/AC ratios, additional tests were carried out with molar ratios higher than 1.5, while keeping the other parameters as constant at the aforementioned optimum values (namely, reaction temperature: 400 °C; catalyst amount: 5 g; O_2/AC ratio: 3.5). The results are presented in Table 4. For NH_3/AC ratios higher

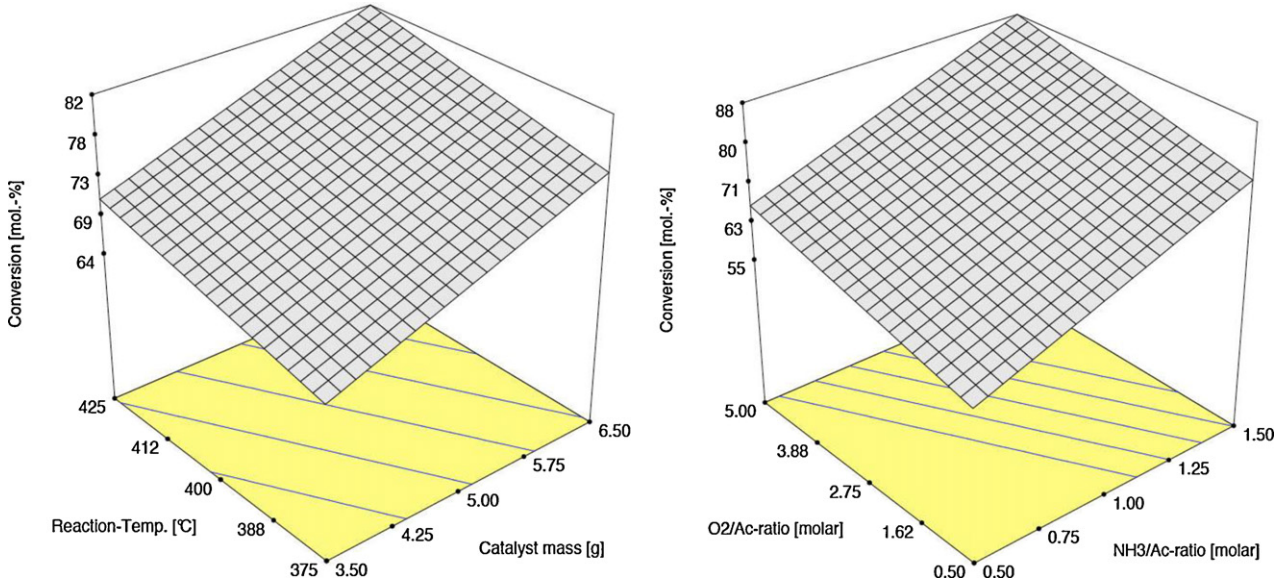

Fig. 2. AC conversion as a function of the reaction temperature and the catalyst amount at constant O_2/AC ratio of 3.5 and NH_3/AC ratio of 1.0 (left); AC conversion as a function of the O_2/AC and NH_3/AC ratios at constant reaction temperature of 400 °C and catalyst amount of 5.0 g (right).

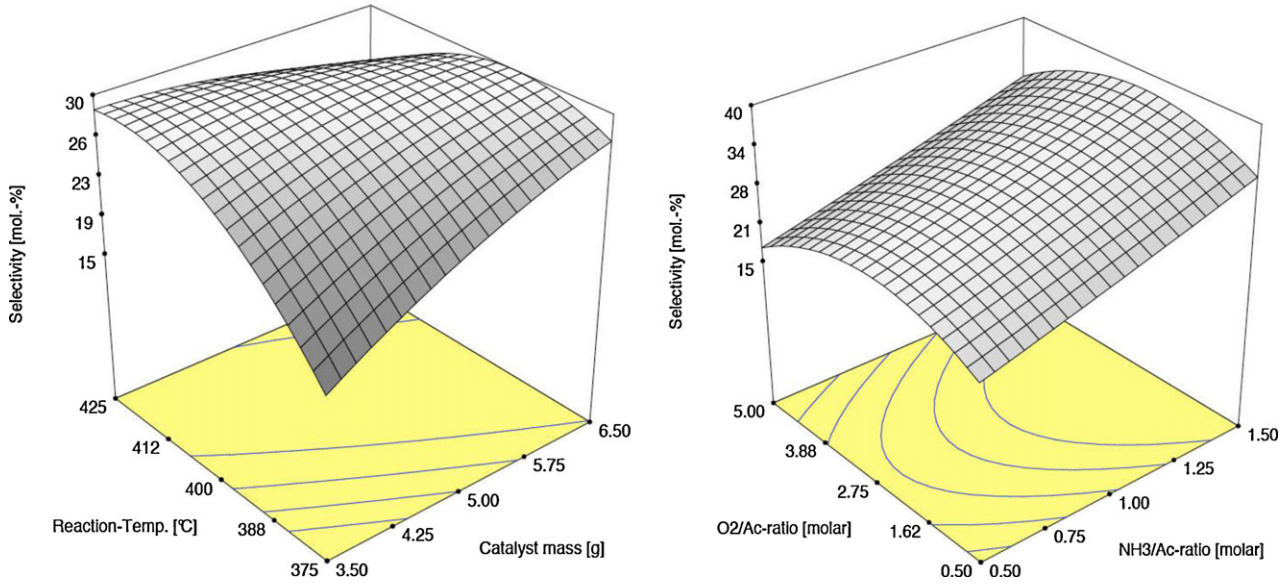

Fig. 3. ACN selectivity as a function of the reaction temperature and catalyst amount at constant O_2/AC ratio of 3.5 and NH_3/AC ratio of 1.0 (left); ACN selectivity as a function of the O_2/AC and the NH_3/AC ratios at constant reaction temperature of 400 °C and catalyst amount of 5.0 g (right).

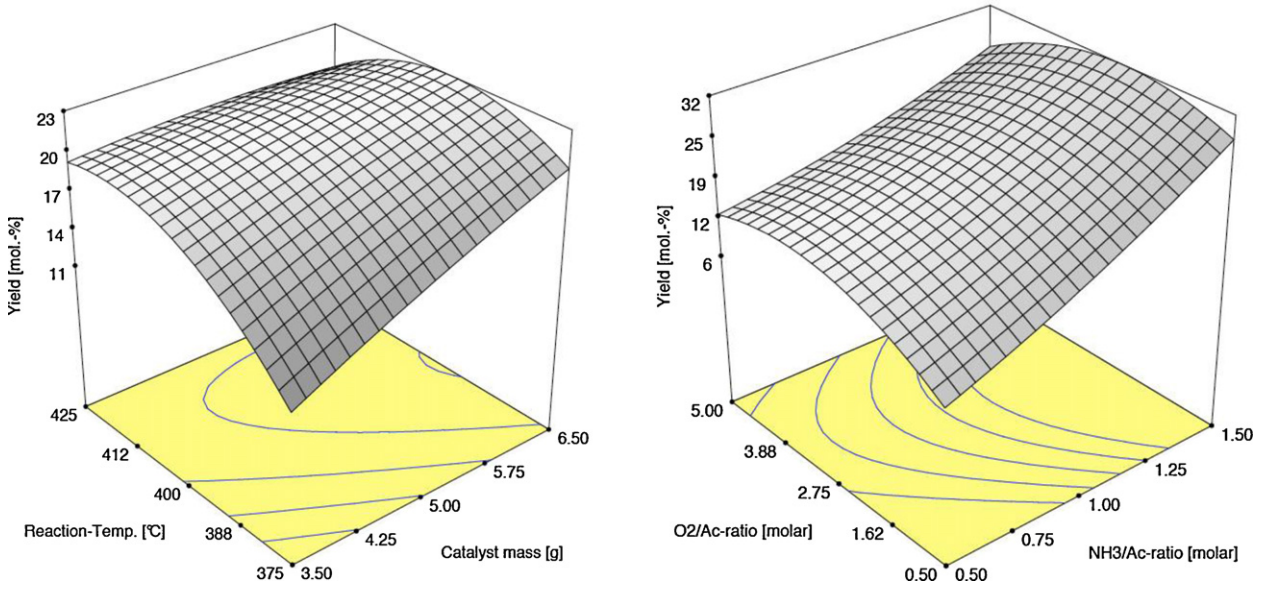

Fig. 4. ACN yield as function of the reaction temperature and catalyst amount at constant O_2/AC ratio of 3.5 and NH_3/AC ratio of 1.0 (left); ACN yield as a function of the O_2/AC and the NH_3/AC ratios at constant reaction temperature of 400 °C and catalyst amount of 5.0 g (right).

than 1.5, the conversion increased from 81% to 88–89%, while the ACN selectivity dropped to 34% ± 1%. This led to a lower yield in ACN, with a decrease from 36% for an NH_3/AC molar ratio of 1.5 to 29% for an NH_3/AC molar ratio of 2. It can be assumed that the increase in AC conversion is caused by a NH_3 induced polymerization of acrolein as described in the literature [42,43]. As reported by Hank et al., already small amounts of NH_3 (AC/NH_3 molar ratio 10,000) are sufficient to promote a polymerization of acrolein [43]. Thus, an NH_3/AC molar ratio of 1.5 was kept as the optimal one.

Table 4
Catalytic performance of SbFeO0.6 for different NH_3/AC ratios.

Catalyst	NH_3/AC	Conversion, %	Selectivity, %	Yield, %	Mass balance, %
		AC	ACN	ACN	
Sb/Fe0.6	1.5	81	44	36	99.0
Sb/Fe0.6	1.75	89	36	32	98.0
Sb/Fe0.6	2	88	33	29	98.0

Reaction temperature 400 °C; catalyst amount 5.0 g; reactant ratio O_2/AC 3.5.

After the reaction screening for the purpose of complying with the design of experiments needs for parameters scanning was completed, point prediction was conducted in order to control if the predicted catalytic performance for the optimized reaction parameters (Fig. 4; reaction temperature of 400 °C, 5.0 g of catalyst, O_2/AC ratio of 3.5, NH_3/AC ratio of 1.5) fits the results of the real experiment under these reaction conditions. Table 5 depicts the catalytic performance obtained in the experiment and the AC conversion, ACN selectivity and ACN yield predicted by the statistical software for the optimized parameters. From the results, one can see that the

Table 5
Comparison of predicted and real results for optimized parameters.

Catalyst	Experiment	Conversion, % ACN	Selectivity, % ACN	Yield, % ACN
Sb/Fe0.6	Predicted	81	37	31
Sb/Fe0.6	Measured	84	44	36

Reaction temperature 400 °C; catalyst amount 5.0 g; reactant ratio O_2/AC 3.5, NH_3/AC 1.5; gas phase composition at 400 °C: 86.8% H_2O, 7.7% O_2, 3.3% NH_3, 2.2% AC.

catalytic performance experimentally obtained is slightly higher than the performance suggested by the software (36% yield *vs.* 31% yield). Nevertheless, the difference is negligible, as the yield observed in the experiment is within the accuracy limitations of the prediction (5% standard error).

3.1.2.4. Influence of water. Water is the main component of the feed for the ammoxidation of acrolein and, in contrast with most of the previous papers dealing with this reaction, the water content in our case is comparatively high (*ca.* 87%). Nevertheless, one can consider that, in an industrial process, the products from the first reactor can be partly purified by condensing the high boiling point intermediates such as hydroxyacetone (boiling point of 145 °C) together with water, before being fed to the second reactor. Thus, the influence of water on the catalytic performance of SbFeO0.6 has been investigated by replacing water in the feed with nitrogen, which was saturated with the appropriate amount of AC. The results obtained in the presence and the absence of water over SbFeO0.6 are presented in Fig. 5.

The acrolein conversion increased during the first 3 h of TOS from 73% to 87% in the experiment without water addition. Afterwards, the conversion stabilized at 85%. In contrast, the AC conversion decreased from 84% (1 h) to 76% (3 h) and remained constant until the end of the experiment when water was present in the solution feed.

The acrylonitrile selectivity remained stable at 26% in the beginning of the experiment without water and started to decrease after 3 h on stream to 21%, ultimately. In contrast, the presence of water significantly increased the selectivity towards the desired product acrylonitrile steadily over time on stream from 29% (1 h) to 47% (2 h) and 52% (3 h).

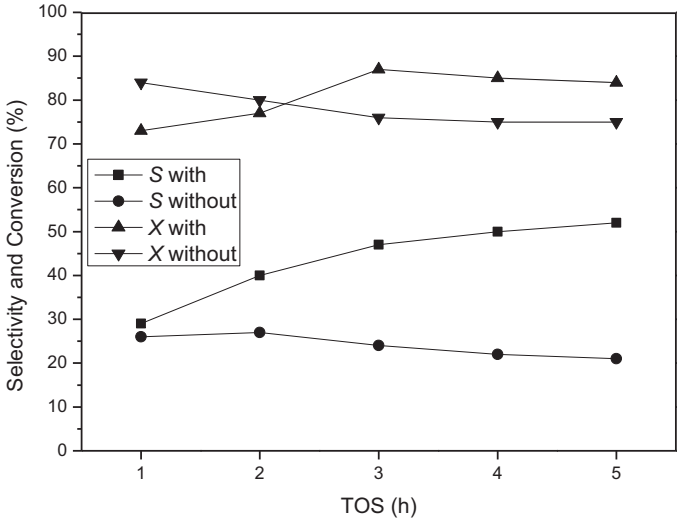

Fig. 5. AC conversion and ACN selectivity plotted over time on stream in the presence and the absence of water at 400 °C, NH_3/AC ratio = 1.5, O_2/AC ratio = 3.5, SbFeO0.6 amount = 5.0 g, contact time = 0.12 s; Gas phase composition at 400 °C: 86.8% H_2O or N_2, 7.7% O_2, 3.3% NH_3, 2.2% AC.

Table 6
Catalytic performance of SbFeO0.6 for different reactants.

Reactant	Hydroxyacetone	Acetaldehyde	Propionaldehyde
Conversion, %	100	74	100
S acrylonitrile, %	0	0	5
S acetonitrile, %	0.5	35	7
S propionitrile, %	–	–	3
S acetaldehyde, %	11	–	4
S acrolein, %	0.1	0.1	5

Reaction temperature 400 °C; catalyst amount 5.0 g; reactant ratio O_2/reactant 3.5, NH_3/reactant 1.5; contact time 0.12 s; 5 h of TOS; gas phase composition at 400 °C: 86.8% H_2O or N_2, 7.7% O_2, 3.3% NH_3, 2.2% reactant.

3.1.2.5. Ammoxidation of by-products. The reactivity of the main by-products of the dehydration of glycerol (hydroxyacetone, acetaldehyde, propionaldehyde; *cf.* Section 3.1.1) under ammoxidation conditions over the WO_3/TiO_2 system were investigated. Therefor, each by-product was used as a reactant in the ammoxidation over SbFeO0.6 under identical reaction conditions as those applied for the ammoxidation of AC. The results are reported in Table 6.

In the case of hydroxyacetone, full conversion and no selectivity towards ACN was observed. The main product identified was acetaldehyde (11%). Only traces of acrolein (0.1%) as well as acetonitrile (0.5%) were found. Due to the high conversion rate, it is most likely that hydroxyacetone was decomposed under the applied reaction conditions into carbon oxides. However, due to technical limitations, identification and quantification of those compounds was not possible.

In the experiment with acetaldehyde, the conversion rate reached 74%. Once again no selectivity towards the desirable product ACN was observed. The main product of the ammoxidation of acetaldehyde was acetonitrile (35%).

Full conversion was obtained in the experiment with propionaldehyde. In contrast to the other reactants, acrylonitrile (5%) was formed under the applied reaction conditions. Furthermore, acrolein (5%), acetaldehyde (4%), propionitrile (3%) and acetonitrile (7%) were identified with similar selectivities. Consequently, from these results, it is suggested that the by-products of the dehydration of glycerol possibly influence the ammoxidation of AC to ACN. Especially, due to formation of propionaldehyde, it is possible that the selectivity towards ACN in the tandem process is even higher than for the single ammoxidation of AC.

The corresponding reactions from the by-products are depicted in Scheme 1.

3.1.2.6. Long-term performance test. The long-term performance of the SbFeO0.6 catalyst has been investigated in a 24 h experiment. The results are shown in Fig. 6.

The acrolein conversion stabilized at 86 ± 1% after 3 h on stream and then remained constant till the end of the experiment. The selectivity towards acrylonitrile increased significantly from 19% (1 h) to 40% (2 h) in the beginning of the experiment. Afterwards, the selectivity increased slightly to 45% (7 h) and remained nearly constant overnight reaching 43% (23 h) and 46% (24 h) at the end of the experiment. Thus, the long-term stability of the antimony iron mixed oxide with a molar ratio of 0.6 was clearly proven.

3.1.3. Tandem ammoxidation of glycerol

3.1.3.1. Adjustment of the residence time in reactor II. Finally, the catalytic performance of the WO_3/TiO_2 catalyst (13.2 wt.%) and of SbFeO0.6 were sequentially investigated in the tandem-reactor. For the dehydration of glycerol to AC, the reaction parameters were selected as those described in Section 2.3. The optimized reaction parameters for the ammoxidation of AC to ACN – obtained

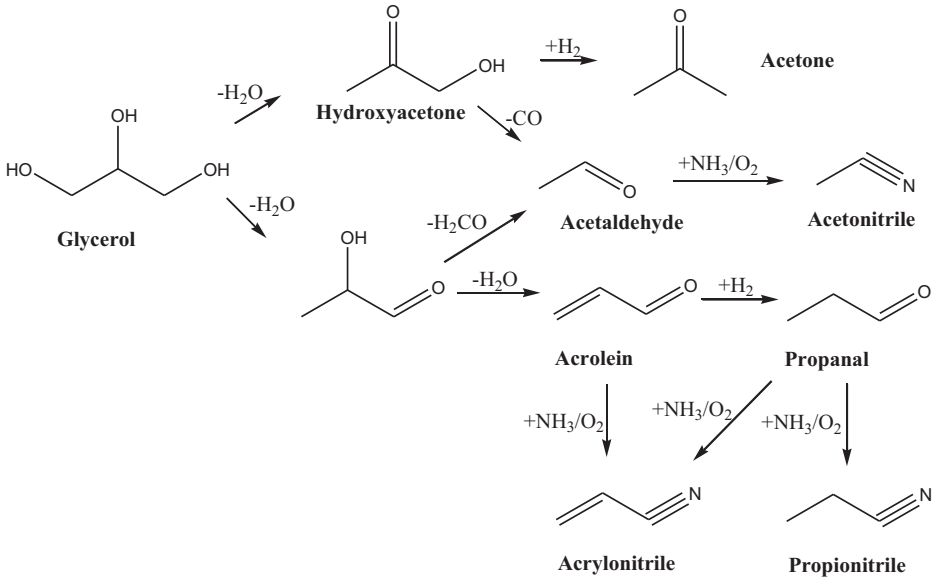

Scheme 1. Ammoxidation reactions of the by-products from the 1st step (dehydration of glycerol).

by the DoE – were adapted to the tandem-reactor (reaction temperature: 400 °C: O_2/AC molar ratio: 3.5; NH_3/AC molar ratio: 1.5) (*cf.* Section 3.1.2.3). However, preliminary experiments with the tandem-reactor showed that the conversion of AC from the first step was significantly lower than expected: 26% of unreacted AC was still detected after the second step compared to an expected value of 14%. One explanation may be that the acrolein concentration in the feed to the second reactor was higher (70% yield in acrolein, *cf.* Section 3.1.1) than the concentration used for the parameter optimization (the concentration corresponded to 62% yield in acrolein, *cf.* Section 2.3).

In order to increase the conversion of acrolein in the ammoxidation step, we thus decided to increase the residence time for the latter reaction. Hence, the catalyst mass was increased by a factor two from 2.75 g to 5.5 g leading to a residence time of 0.24 s (compared to the previous value of 0.12 s). The results are reported in Fig. 7. The conversion of glycerol remained stable at 100% over 6 h on stream. In the first hour on stream, 20% selectivity to ACN was observed. Thereafter, the selectivity stabilized at values above 40%, showing a gently increasing trend. The AC selectivity slightly increased during the first 4 h on stream from 4% to 10% and remained constant afterwards. This suggests that, even with increased residence time of 0.24 s, the conversion of AC in the ammoxidation stage is not complete, which is in agreement with the previous results (Section 3.1.2).

Nevertheless, the overall catalytic performance is significantly higher than that one could expect from the combination of the independent results of the decoupled experiments, which supposed selectivity to AC of 14% and 27% to ACN at 100% glycerol conversion and 81% acrolein conversion, respectively. This result may be explained by the higher amount of catalyst. The mass balance of the experiment was 97.5%.

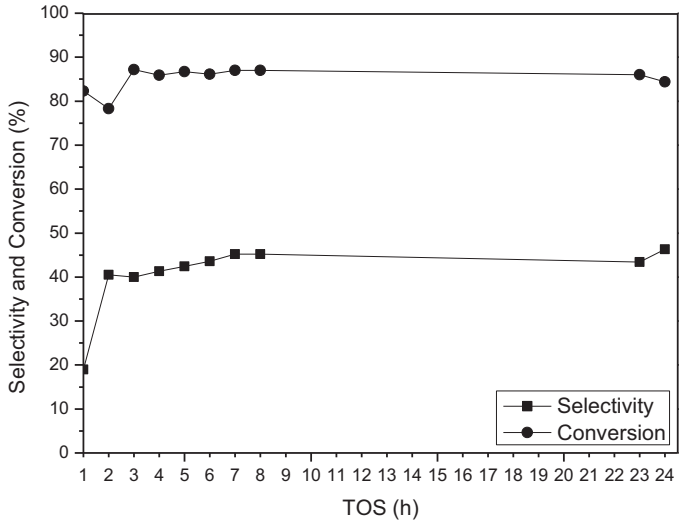

Fig. 6. Catalytic performance of SbFeO0.6 plotted over time on stream; reaction conditions: 400 °C, NH_3/AC ratio = 1.5, O_2/AC ratio = 3.5, catalyst amount = 5.0 g, contact time = 0.12 s; gas phase composition at 400 °C: 86.8% H_2O, 7.7% O_2, 3.3% NH_3, 2.2% AC.

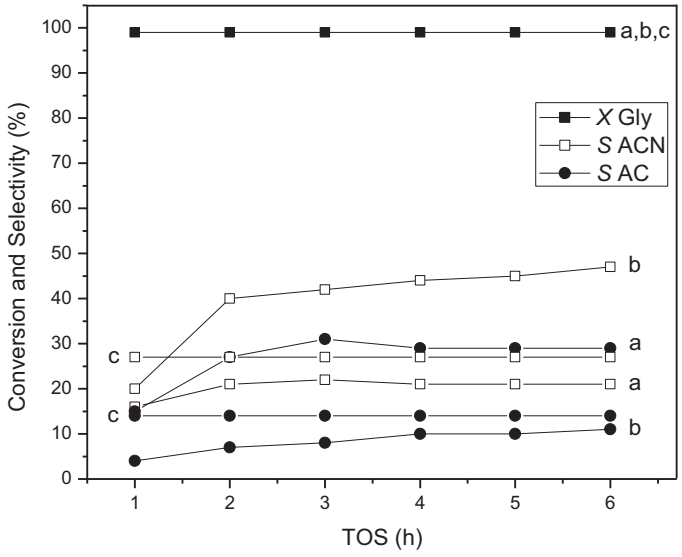

Fig. 7. Catalytic performance as function of time on stream for the combined reactions; a: 2.75 g catalyst step II, b: 5.5 g catalyst step II, c: predicted results; reaction conditions step I: 280 °C, 5.0 g of 13.2 wt.% WO_3/TiO_2 catalyst, O_2/glycerol ratio of 0.6, contact time of 0.36 s, gas phase composition at 280 °C: 92.74% H_2O, 2.72% O_2, 4.54% glycerol and step II: 400 °C, 2.75 g or 5.5 g of SbFeO0.6 catalyst, O_2/AC ratio of 3.5, NH_3/AC ratio of 1.5, contact time of 0.12 s or 0.24 s, gas phase composition at 400 °C: 86.8% H_2O, 7.7% O_2, 3.3% NH_3, 2.2% AC.

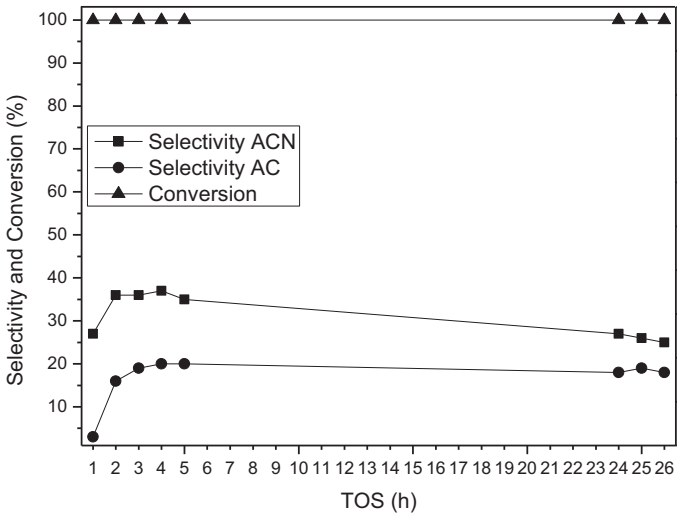

Fig. 8. Catalytic performance as function of time on stream for the combined reactions; reaction conditions step I: 280 °C, 5.0 g of 15 wt.% WO_3/TiO_2 catalyst, O_2/glycerol ratio of 0.6, contact time of 0.36 s, gas phase composition at 280 °C: 92.74% H_2O, 2.72% O_2, 4.54% glycerol and step II: 400 °C, 5.5 g of SbFeO0.6 catalyst, O_2/AC ratio of 3.5, NH_3/AC ratio of 1.5, contact time of 0.24 s, gas phase composition at 400 °C: 86.8% H_2O, 7.7% O_2, 3.3% NH_3, 2.2% AC.

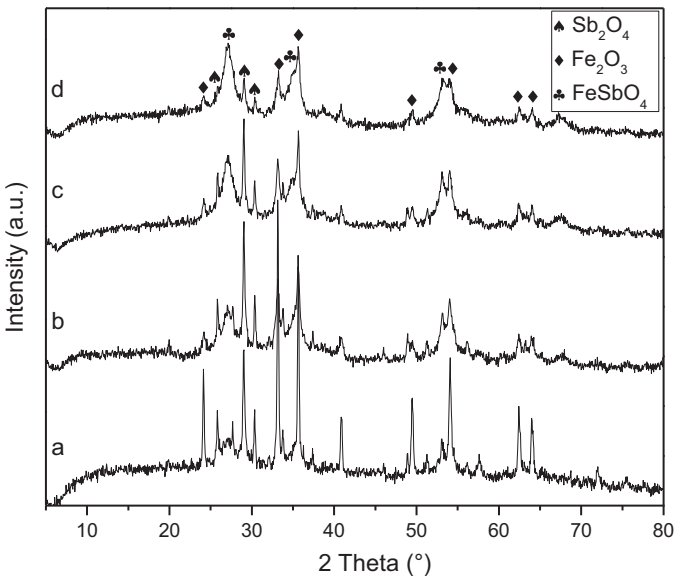

Fig. 9. XRD patterns of the calcined catalysts (a: SbFeO0.4, b: SbFeO0.6, c: SbFeO0.8, d: SbFeO1.0).

3.1.3.2. Long-term performance test. The long-term performance of the indirect ammoxidation of glycerol was studied in a 26 h experiment over a 15 wt.% WO_3/TiO_2 catalyst (step I) and the SbFeO0.6 catalyst (step II). The results are given in Fig. 8.

The glycerol conversion remained stable at 100% over 26 h on stream. The acrylonitrile selectivity increased from 27% (1 h) to 36 ± 1%, and remained stable for the first 5 h on stream. Afterwards, the selectivity steadily decreased to 25% (26 h). The selectivity towards the intermediate acrolein increased from 3% (1 h) over 16% (2 h) to 20 ± 1% and remained constant until the end of the experiment. In contrast to the best performance obtained so far for the indirect ammoxidation of glycerol (40% yield in ACN over 6 h on stream, *cf.* Section 3.1.3.1), the performance over 26 h on stream was clearly decreased. However, regarding only the first 5 h of the experiment, the yield in acrylonitrile was comparable to the best experiment (34% on average *vs.* 40%). In terms of acrolein, the selectivity was more than doubled compared to the best performance observed so far (20% *vs.* 8%). This is most likely caused by the different catalyst batch used for the dehydration in this experiment (15 wt.% WO_3/TiO_2 *vs.* 13.2 wt.% WO_3/TiO_2), which caused probably a higher yield in acrolein in the first step.

Ulgen et al. stated that the glycerol conversion over a similar catalyst (13.9 wt.% WO_3/TiO_2) decreased by 20% after 24 h on stream [15]. This fact may explain the decreasing trend observed for the acrylonitrile selectivity, meaning that the acrolein concentration in the feed to the second reactor decreased over the time on stream. Therefore, the NH_3/AC ratio increased over the time, which led to a decreasing ACN selectivity, as observed by the variation of the NH_3/AC ratio during the experimental design (*cf.* Section 3.1.2.3). Furthermore, the arrival of non-converted glycerol in the second reaction step may affect the catalytic performance. Glycerol will be thermally activated and form – among others – coke (*cf.* Fig. S1). Thus, the ammoxidation catalyst is also deactivated, which results in a decreasing acrolein conversion. Consequently, *i)* the glycerol conversion remains stable at 100%, *ii)* the lower amount of AC in the feed to second reactor is compensated by the lower activity of the ammoxidation catalyst, whereby the selectivity towards AC in total is constant and *iii)* due to the deactivation of SbFeO0.6, the selectivity to ACN drops.

3.2. Characterization results and interpretation of the catalytic performances

The SbVO and SbFeO catalysts were characterized using various techniques in order to explain the differences in conversion and selectivity to the respectively desired products.

3.2.1. XRD

The catalysts were characterized by X-ray diffraction to study the relationship between the different phases observed over the mixed oxides and catalytic performances.

The results of the X-ray diffraction of the SbFeO catalysts with different molar ratios are presented in Fig. 9. Three different phases were identified in all the catalysts: antimony-IV-oxide, iron-III-oxide and iron-antimony mixed oxide. The characteristic peaks of Sb_2O_4 were identified at 2θ = 25.8°, 29°, 30.3° (JCPDS #11-0694) and those of Fe_2O_3 at 2θ = 24.2°, 33.2°, 35.7°, 49.4°, 54°, 62.4°, 64° (JCPDS #33-0664). The characteristic reflections of the antimony iron mixed oxide phase $FeSbO_4$ were present at 2θ = 27.2°, 34.9°, 53.1° (JCPDS #34-0372).

From the comparison of the four catalysts with different ratios, one can see that – as expected – the FeSbO catalyst with iron excess (molar Sb/Fe ratio of 0.4) shows the highest iron-III-oxide reflexion intensity. Afterwards, the intensity of these peaks decreases with an increasing antimony amount. Nevertheless, the signal of Fe_2O_3 is still detectable even in the case of the stoichiometric Sb/Fe molar ratio of 1.0, meaning that iron and antimony do not quantitatively form the mixed oxide ($FeSbO_4$). This could also be confirmed by looking at the peaks related to antimony dioxide. These latter exhibit a comparable level for the mixed oxides with the molar ratios 0.4 and 0.6. However, the signal intensity decreases for the catalysts with a higher antimony content (SbFeO1.0 and SbFeO0.8), but still remains detectable. As the characteristic reflections of the antimony iron mixed oxide $FeSbO_4$ became sharper with an increasing antimony amount, it can be concluded that the decrease in intensity of the characteristic peaks of Sb_2O_4 is caused by the enhanced formation of the $FeSbO_4$ mixed phase. This means the higher the Sb/Fe ratio of the bulk catalyst, the more $FeSbO_4$ is formed. Nevertheless, one cannot exclude that the decrease in intensity might also be caused by the formation of an amorphous

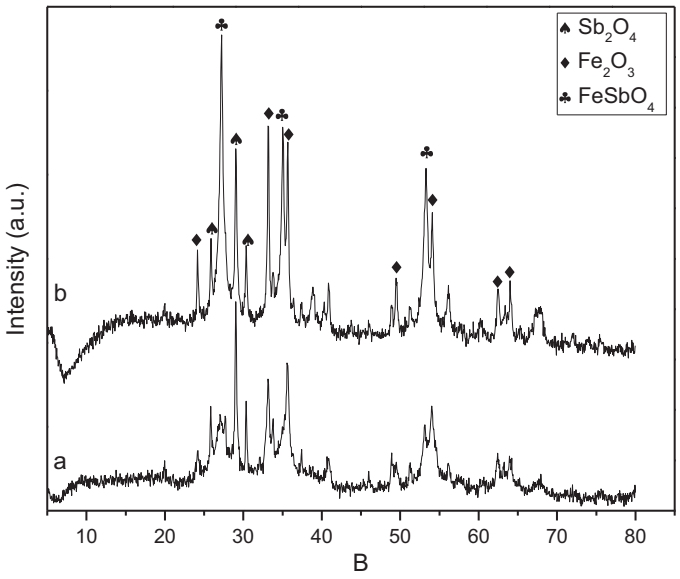

Fig. 10. XRD patterns of the fresh (a) and spent (b) SbFeO0.6.

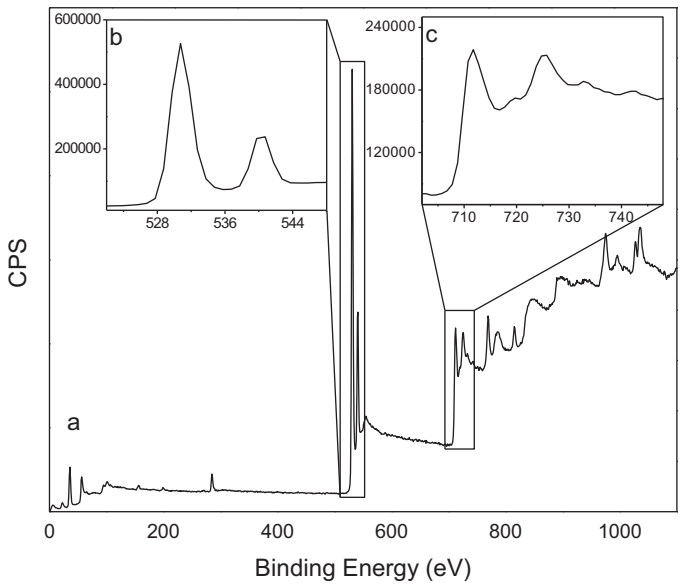

Fig. 11. XPS spectra of SbFeO0.6: (a) wide scan of SbFeO0.6 showing principal transitions, (b) Sb3d/O1s region, (c) Fe2p region.

phase, even though, no such example was reported in the literature yet.

To study the influence of the reaction conditions on the crystalline structure of the catalyst, the spent antimony-iron catalysts with molar ratios of 0.4 and 0.6 were analysed by XRD. The diffraction patterns of the fresh and spent catalyst are given in Fig. 10 and Fig. S3. All the phases (Sb_2O_4, Fe_2O_3, $FeSbO_4$) that were already found in the calcined catalysts were also identified in the spent catalysts.

Nevertheless, when comparing the XRD pattern of the fresh and spent FeSbO with a molar ratio of 0.6, one can clearly realize that the intensity of the characteristic reflections of the antimony-iron mixed oxide ($FeSbO_4$) were increased after the reaction. Thus, it is assumed that additional crystalline mixed phase is formed under reaction conditions. Furthermore, the broadness of the peaks was significantly decreased after reaction, suggesting thus an increase in the crystallites size–supposedly due to sintering. On the other hand, the pattern of the catalyst with a molar ratio of 0.4 remained unchanged during the experiment (*cf.* Fig. S3). In fact, no change of the respective intensity for the three identified phases was observed.

This *in situ* formation of the crystalline $FeSbO_4$ phase can be directly correlated with the observed increase in selectivity during the first 3 h on stream observed for the SbFeO catalysts with molar ratios of 0.6, 0.8 and 1.0 (*cf.* Section 3.1.2.2). Thus, it is supposed that the mixed phase $SbFeO_4$ is the active species.

On the other hand, the selectivity to ACN observed in the experiment with SbFeO0.4 even decreased over the time as no additional $FeSbO_4$ was found after test–most likely due to the low antimony content in the bulk, making the *in operando* formation impossible (*cf.* Section 3.1.2.2).

3.2.2. XPS

To support the results obtained by XRD (*cf.* Section 3.2.1), which suggests the formation of the $SbFeO_4$ mixed phase during test, XPS investigations were performed. Fig. 11a shows the X-ray photoelectron spectrum of the fresh SbFeO catalyst with a molar ratio of 0.6. The peaks at 22 eV, 400 eV, 540 eV and 710–711 eV correspond to the characteristic binding energies of O2s, N1s, $Sb3d_{3/2}$ and $Fe2p_{3/2}$. The peaks of O1s and $Sb3d_{5/2}$ overlap at 531 eV. Therefore, it was necessary to use the O2s and the $Sb3d_{3/2}$ peaks to carry out the quantification of antimony. All the other peaks can be assigned to photoemission and Auger transitions of iron, antimony and oxygen.

The Sb $3d_{3/2}$ peak magnified in Fig. 11b may correspond to a 5+ oxidation state of antimony. However, it is known from the literature that the identification of the antimony oxidation state can be difficult as the binding energy of Sb^{3+} and Sb^{5+} only differs by 0.6 eV [44]. Therefore, we could not clearly distinguish between the two oxidation states from our XPS results. This issue has been previously discussed in the literature, which suggests the existence of a surface layer containing only Sb^{5+} [45] as well as a mixture of Sb^{3+} and Sb^{5+} [46,47]. The $Fe2p_{3/2}$ peak located in the 710 eV to 711 eV range (Fig. 11c) is comparable to values recorded for Fe_2O_3, thus showing that iron is exclusively present at the oxidation state 3+.

Furthermore, the presence of Sb^{5+} and Fe^{3+} proves that the $FeSbO_4$ mixed phase is present at surface of the catalyst [48].

The surface ratio of antimony to iron was calculated using data from the $Sb3d_{3/2}$ and the $Fe2p_{3/2}$ peaks. The results of the calcined FeSbO catalysts with molar ratios from 0.4 to 1.0 are shown in lines one, two, four and five in Table 7, respectively. The atomic Sb/Fe ratio at the surface of the catalyst increased with the antimony loading from 0.16 to 1.50. However, the as-determined antimony to iron ratios at the surface never matched those from the theoretical bulk catalysts.[1] In fact, whereas the catalysts with molar ratios of 0.4 and 0.6 showed an excess in iron at their surface with atomic ratios of 0.16 and 0.33, respectively, an enrichment in antimony at the surface was observed for FeSbO0.8 and FeSbO1.0, with ratios of 1.25 and 1.5, respectively (Fig. 12). With respect to the results of the catalytic experiments, no direct correlation between the AC conversion and the Sb/Fe surface ratio can be found. From research on the ammoxidation of propene and propane, it is known that the role of antimony is to activate the hydrocarbon [49]. Additionally, it is reported that an excess in antimony at the catalyst surface improves the selectivity to ACN [45,49]. Though, the results obtained in our study do not support this suggestion (*cf.* Section 3.1.2.2). The role of iron is predominantly the Fe^{2+}/Fe^{3+} redox couple that enables the oxygen adsorption and activation [49].

[1] Elemental analysis by ICP of the catalysts was impossible, as the catalysts did not dissolve even in HF after several weeks.

Table 7
Surface analysis results of the calcined and spent SbFeO catalysts.

No.	Catalyst	Condition	Binding energy, eV		Atomic conc., %		Atomic ratio
			Sb $3d_{(3/2)}$ (Sb^{5+})	Fe $2p_{(3/2)}$ (Fe^{3+})	Sb	Fe	Sb/Fe
1	SbFeO0.4	Calcined	540.5	711.1	4	25	0.16
2	SbFeO0.6	Calcined	540.6	711.5	7	21	0.33
3	SbFeO0.6	Spent	540.6	711.5	13	10	1.30
4	SbFeO0.8	Calcined	540.5	711.4	15	12	1.25
5	SbFeO1.0	Calcined	540.4	710.8	15	10	1.50

Catalyst mentioned in line 3 spent at reaction temperature 400 °C; catalyst amount 5.0 g; reactant ratio O_2/AC 0.5; NH_3/AC 1.0; contact time of 0.12 s; gas phase composition at 400 °C: 94% H_2O, 1.2% O_2, 2.4% NH_3, 2.4% AC

Table 8
Textural properties of the calcined and spent SbFeO and SbVO catalysts.

No.	Catalyst	Condition	S_{BET}, m^2/g	$S_{Micro\ BET}$, m^2/g	V_P, cm^3/g	$V_{Micro\ P}$, cm^3/g	Productivity, mmol ACN/h m^2
1	SbFeO0.4	Calcined	20	2	0.06	0.0005	0.094
2	SbFeO0.6	Calcined	24	5	0.08	0.002	0.080
3	SbFeO0.6	Spent	14	0	0.04	0	0.135
4	SbFeO0.8	Calcined	32	3	0.11	0.001	0.094
5	SbVO0.8	Calcined	2	1	0.01	0.0004	0.640
6	SbFeO1.0	Calcined	19	2	0.07	0.0005	0.062

Catalyst mentioned in line 3 spent at reaction temperature 400 °C; catalyst amount 5.0 g; reactant ratio O_2/AC 0.5; NH_3/AC 1.0; contact time 0.12 s; gas phase composition at 400 °C: 94% H_2O, 1.2% O_2, 2.4% NH_3, 2.4% AC

The effect of the reaction conditions on the catalyst has also been studied by XPS. In the case of the catalysts with Sb/Fe ratio higher than 0.4, XRD of the spent catalyst exhibited increased amount of the SbFe-mixed oxide phase, (*cf.* Section 3.2.1). The results of the XPS of the spent SbFeO with a molar ratio of 0.6 are presented in line three in Table 7. The antimony to iron atomic ratio considerably increased during the experiment from 0.33 to 1.3. Allen et al. stated that an enrichment of Sb at the surface of the catalyst is probably caused by the formation of the $FeSbO_4$ phase as already suggested by XRD (*cf.* 3.2.1). The termination of the $FeSbO_4$ lattice is such that antimony cations dominate at the surface region [48]. Thus, one can assume that the $FeSbO_4$ mixed phase is formed under the conditions used for the catalytic experiments as it was already stated from the XRD results for the spent $FeSbO_4$ with a molar ratio of 0.6 (*cf.* Section 3.2.1).

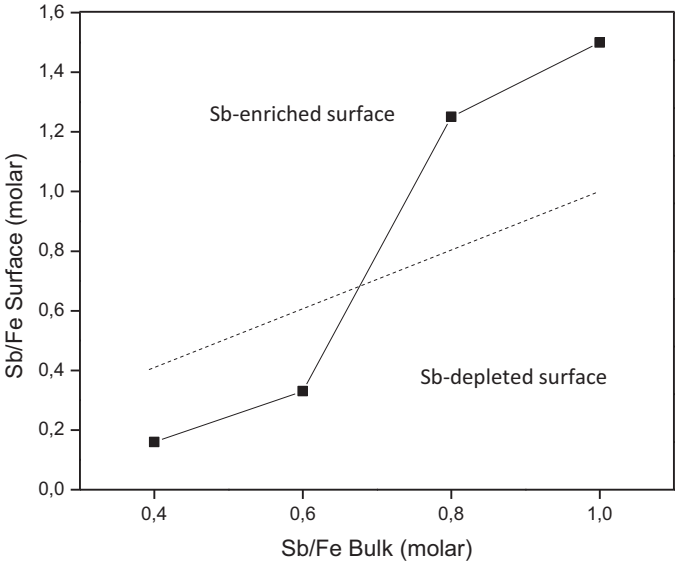

Fig. 12. Surface Sb/Fe ratio as a function of the bulk Sb/Fe ratio.

3.2.3. Nitrogen physisorption

The influence of the different compositions of the catalysts on their textural properties was investigated by nitrogen physisorption. The results of the nitrogen physisorption/desorption measurements of the SbVO and SbFeO catalysts with molar ratios of 0.8 are reported in lines four and five in Table 8. The antimony-vanadium catalyst exhibited a significantly lower specific surface area with 2 m^2/g than the antimony-iron catalyst having 32 m^2/g. Nevertheless, this discrepancy in the specific surface area did not yield any impact in terms of catalytic conversion, as both catalysts exhibited nearly the same conversion level of AC with values of 80% and 75%, respectively (*cf.* Section 3.1.2.1).

The specific surface area of antimony-iron catalysts with different molar ratios was then checked. The results reported in lines one, two, four and six in Table 8 show that the specific surface area initially increases with the atomic Sb/Fe ratio from 20 m^2/g (SbFeO0.4) to 32 m^2/g (SbFeO0.8) but afterwards drops to 19 m^2/g (SbFeO1.0). The pore volume showed a similar trend as it increased from 0.06 to 0.11 cm^3/g before decreasing to 0.07 cm^3/g. With respect to the catalytic conversion observed for those catalysts, one can see that the AC conversion follows the same trend as the surface area of the SbFeO catalysts with molar ratios of 0.6, 0.8 and 1.0. However, the conversion of SbFeO0.4 does not fit into this sequence, as it is the second highest conversion of all the tested catalysts (70%). Furthermore, the obtained yield in ACN does not directly correlate with the observed development of the surface area of the catalysts (*cf.* Section 3.1.2.2) either. However, the catalyst with the highest surface area (SbFeO0.8, 32 m^2/g) provides the highest yield in ACN of 25%.

In the last series, the SbFeO catalyst with a molar ratio of 0.6 was also exemplarily analysed after test. The result is reported in line 3 in Table 8. The specific surface area as well as the pore volume of the catalyst decreased by roughly a factor two during the reaction, reaching 14 m^2/g and 0.04 cm^3/g respectively after test (compared with 24 m^2/g and 0.08 cm^3/g for the fresh catalyst). Furthermore, the micropores surface area decreased from 5 m^2/g to 0 m^2/g during the reaction. This decrease can be explained by sintering (as also suggested by XRD – *cf.* Section 3.2.1) as well as by the formation of carbonaceous compounds in the micropores of the catalyst during the reaction. Nevertheless, as the catalytic performance after 1 h on stream remained rather stable during the long-term test of 24 h,

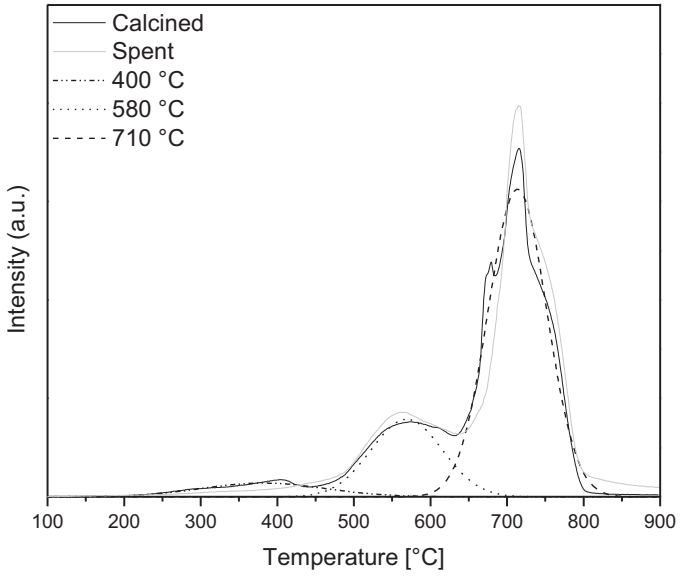

Fig. 13. TPR profile of the calcined (black) and spent (grey) SbFeO0.6.

one can assume that the carbonaceous deposits are rather located in the micropores and a so-to-speak steady state is then reached when the latter are blocked.

3.2.4. TPR

Finally, FeSbO0.6 was studied by H_2-TPR to analyse the reducibility of the different phases of the mixed oxide catalyst before and after test. The H_2-TPR profiles of the calcined and spent catalyst are shown in Fig. 13. No significant difference was observed for the calcined and spent catalyst. Both samples exhibited identical reduction bands at 400 °C, 580 °C and 710 °C.

It has been reported by de Abreu et al. that the reduction of Fe_2O_3 to Fe_3O_4 in the presence of H_2 takes place at 400 °C [50]. Therefore, it can be safely assumed that the reduction band at 400 °C of FeSbO0.6 is caused by the reduction of iron as the Fe_2O_3 phase was identified by XRD (*cf.* Section 3.2.1). The reduction band with a maximum at 580 °C was assigned to a reduction of the $FeSbO_4$ phase [51,52]. Bithell et al. showed that, under reducing conditions at temperatures of 350 °C to 500 °C, a phase separation of $FeSbO_4$ occurs, in which an antimony oxide is formed [51].

Van Steen et al. observed a similar phenomenon–It was stated that, at 650 °C isothermal conditions, $FeSbO_4$ decomposes to Sb_2O_3 and Fe_2O_3. However, the applied reducing conditions are different for this TPR study [52]. The highest H_2 consumption was observed at temperatures in the range of 600–800 °C. The shape of the reduction band implies that several reduction processes interfere with each other. It is suggested that the reduction of Fe_3O_4 to Fe^0 occurs simultaneously to the reduction of Sb_2O_4 to Sb_2O_3 [50,53].

The TPR results of the spent SbFeO0.6 illustrate that the catalyst was neither reduced nor oxidized during the reaction, as the TPR profiles of the calcined and spent catalyst show only marginal differences. Nevertheless, it depends on the concentration of reducing agent (NH_3) and oxidizing agent (O_2) in the feed of the reactor if a reduction may take place. From the TPR results, one could suggest that a reduction of Fe_2O_3 is possible at the reaction temperature of 400 °C, but this would necessitate large excess in ammonia. However, the XRD diffractogram of the spent FeSbO0.6 proves that no Fe_3O_4 was formed during the experiment (*cf.* Section 3.2.1). Hence, it can be concluded that the ammonia concentration was too low to enable a reduction of iron-III to iron-II. Additionally, the reduction of Sb_2O_4 or $FeSbO_4$ under the applied reaction conditions can be ruled out since the reaction temperature was insufficient. Nevertheless, the results imply that the reaction conditions have to be chosen carefully in order to avoid the decomposition of the $FeSbO_4$ active species during reaction.

4. Conclusions

The indirect ammoxidation of glycerol to acrylonitrile was studied using a WO_3/TiO_2 catalyst for the dehydration of glycerol to acrolein and Sb-V-O or Sb-Fe-O catalysts for consecutive ammoxidation of this latter. Sb-Fe-O catalysts proved to be more efficient for the second step and our work revealed that the Sb/Fe ratio has a significant influence on the catalytic performance in the ammoxidation of acrolein, whereby ratios of 0.6 and 0.8 were found most favourable. The best result with 44% selectivity in ACN at 81% AC conversion (36% yield in ACN) was obtained over a FeSbO catalyst with a molar ratio of 0.6 at 400 °C, with 5 g of catalyst, an NH_3/AC ratio of 1.5 and, an O_2/AC ratio of 3.5 and a contact time of 0.24 s. The results of the nitrogen physisorption imply that no correlation between the catalytic activity and the surface area or the pore volume can be determined. Evidence was found by X-ray diffraction that additional $FeSbO_4$ is formed under reaction conditions, which was correlated to an increase in selectivity towards ACN in the first 3 h time on stream. This result was further confirmed by XPS analysis. The XPS study of the spent FeSbO catalyst with a bulk molar ratio of 0.6 showed that the Sb/Fe ratio at the catalyst surface considerably increased under reaction conditions, which was assigned to the formation of the $FeSbO_4$ phase. A long-term experiment revealed that the catalytic performance remained constant after 7 h of time on stream. This indicates that the formation of $FeSbO_4$ under reaction conditions is a time-limited process (induction phase).

The results from TPR of the FeSbO catalyst with a molar ratio of 0.6 suggest that the reduction of the Fe_2O_3 phase to Fe_3O_4 is possible at the reaction temperature of 400 °C in the case of high NH_3 concentrations. However, the XRD of the spent SbFeO0.6 did not show any evidence for formation of Fe_3O_4. Furthermore, the TPR results suggest that decomposition of the $FeSbO_4$ phase into Sb_2O_3 and Fe_2O_3 is possible at 400 °C in the presence of a sufficient reductive environment. Therefore, the reaction conditions have to be advisedly selected – especially the ammonia and oxygen concentration in the feed – in order to avoid the destruction of the desirable $FeSbO_4$ phase, which is the active phase.

Finally, the feasibility of the indirect ammoxidation of glycerol to acrylonitrile with the intermediate formation of acrolein was proven in a tandem-reactor setup. In the experiment over the 13.2 wt.% WO_3/TiO_2 catalyst (step I) and the FeSbO catalyst with a molar ratio of 0.6 (step II), a yield of 40% in ACN was observed (100% glycerol conversion and 40% selectivity to ACN). The long-term performance of the indirect ammoxidation of glycerol mainly depends on the dehydration catalyst lifetime. The yield in ACN dropped by 10% over 24 h TOS due to an increasing NH_3/AC ratio caused by the deactivation of the dehydration catalyst, which led to a decreasing AC concentration in the feed to the second reactor. Additionally, the arrival of non-converted glycerol in the second reactor led to the formation of carbonaceous compounds, which resulted in a deactivation of the SbFeO0.6 catalyst.

Acknowledgements

The research leading to these results has received funding from the European Union Seventh Framework Programme (FP7/2007–2013) under grant agreement no. 241718 EuroBioRef. A part of that research was carried out at TCHK at Aachen University.

We also thank Sachtleben AG for providing the TiO_2.

The authors furthermore thank Mr. O. Gardoll, Mr. A. Beaurain and Mr. G. Cambien for TG, TPR, XPS and BET measurements.

The “Fonds Européen de Développement Régional (FEDER)”, “CNRS”, “Région Nord-Pas-de-Calais” and “Ministère de l‘Education Nationale de l‘Enseignement Supérieur et de la Recherche” are also acknowledged for fundings of X-ray diffractometers.

Appendix A. Supplementary data

Supplementary data associated with this article can be found, in the online version, at http://dx.doi.org/10.1016/j.apcatb.2012.11.035.

References

[1] BP Energy Outlook 2030, BP Energy Outlook 2030, 2012, http://www.bp.com/sectiongenericarticle800.do?categoryId=9037134&contentId=7068677
[2] B.M.E. Russbueldt, W.F. Hoelderich, Journal of Catalysis 271 (2010) 290–304.
[3] Directive 2009/28/EC of the European Parliament and of the council of 23 April 2009 on the promotion of the use of energy from renewable sources and amending and subsequently repealing Directives 2001/77/EC and 2003/30/EC.
[4] European Biodiesel Board, 2012, http://www.ebb-eu.org
[5] R. Christoph, B. Schmidt, U. Steinberner, W. Dilla, R. Karinen, Glycerol, Ullmann's Encyclopedia of Industrial Chemistry.
[6] B. Katryniok, S. Paul, M. Capron, C. Lancelot, V. Bellière-Baca, P. Rey, F. Dumeignil, Green Chemistry 12 (2010) 1922.
[7] J. ten Dam, U. Hanefeld, ChemSusChem 4 (2011) 1017–1034.
[8] M. Pagliaro, R. Ciriminna, H. Kimura, M. Rossi, C. Della-Pina, Angewandte Chemie International Edition 46 (2007) 4434.
[9] M. Pagliaro, R. Ciriminna, H. Kimura, M. Rossi, C. Della-Pina, European Journal of Lipid Science and Technology 111 (2009) 788.
[10] M. Pagliaro, M. Rossi, The Future of Glycerol: New Uses of a Versatile Raw Material, 2nd edition, RSC Green Chemistry Book Series, 2011.
[11] C.-J. Jia, Y. Liu, W. Schmidt, A.-H. Lu, F. Schüth, Journal of Catalysis 269 (2010) 71–79.
[12] H. Redlingshöfer, C. Weckbecker, K. Huthmacher, A. Dörflein, WO 2008/092533 (Evonik Degussa GmbH), 2008.
[13] E. Tsukuda, S. Sato, R. Takahashi, T. Sodesawa, Catalysis Communications 8 (2007) 1349–1353.
[14] J. Deleplanque, J.L. Dubois, J.F. Devaux, W. Ueda, Catalysis Today 157 (2010) 351–358.
[15] A. Ulgen, W.F. Hoelderich, Applied Catalysis A: General 400 (2011) 34–38.
[16] B. Katryniok, S. Paul, V. Bellière-Baca, P. Rey, F. Dumeignil, Green Chemistry 12 (2010) 2079.
[17] B. Katryniok, S. Paul, M. Capron, F. Dumeignil, ChemSusChem 2 (2009) 719–730.
[18] B. Katryniok, S. Paul, M. Capron, V. Bellière-Baca, P. Rey, F. Dumeignil, ChemSusChem 5 (2012) 1298–1306.
[19] J.-L. Dubois, C. Duquenne, W. Hölderich, FR 2884817, (Arkema), 2005.
[20] J.-L. Dubois, C. Duquenne, W. Hölderich, FR 2884818, (Arkema), 2006.
[21] J.-L. Dubois, C. Duquenne, W. Hölderich, J. Kervennal, FR 2882053, (Arkema), 2005.
[22] Y.T. Kim, K.D. Jung, E.D. Park, Microporous and Mesoporous Materials 131 (2010) 28–36.
[23] Y.T. Kim, K.D. Jung, E.D. Park, Applied Catalysis B: Environmental 107 (2011) 177.
[24] Y.T. Kim, K.D. Jung, E.D. Park, Applied Catalysis A: General 393 (2011) 275.
[25] A. Alhanash, E.F. Kozhevnikova, I.V. Kozhevnikov, Applied Catalysis A: General 378 (2010) 11.
[26] D. Arntz, A. Fischer, M. Höpp, S. Jacobi, J. Sauer, T. Ohara, T. Sato, N. Shimizu, H. Schwind, Acrolein, Ullmann's Encyclopedia of Industrial Chemistry.
[27] F.J. Bellringer, T. Bewley, H.M. Stanley, GB 709337, (Distillers), 1951.
[28] J.-L. Dubois, in: Arkema (Ed.), US 2010/0048850, (Arkema) (2010).
[29] H. Oka, K. Miyake, Y. Harano, T. Imoto, Journal of Applied Chemistry and Biotechnology 25 (1975) 663–670.
[30] J.F. Bradzil, Acrylonitrile, Kirk-Othmer Encyclopedia of Chemical Technology.
[31] J.D. Idol, US 2904580, (The Standard Oil Company) (1959).
[32] W.R. Knox, K.M. Taylor, G.M. Tullman, US 3833638, (Monsanto) (1974).
[33] M.O. Guerrero-Perez, M.A. Banares, ChemSusChem 1 (2008) 511–513.
[34] V. Calvino-Casilda, M.O. Guerrero-Pérez, M.A. Bañares, Applied Catalysis B: Environmental 95 (2010) 192–196.
[35] A. Ulgen, W. Hoelderich, Catalysis Letters 131 (2009) 122–128.
[36] F. Wang, J.-L. Dubois, W. Ueda, Applied Catalysis A: General 376 (2010) 25–32.
[37] B. Wood, Production of unsaturated aliphatic nitriles, GB 897226, (Distillers), 1962.
[38] H. Vanderborght, Proceïdeï de preparation de nitriles non satureïs, BE 628287, (UCB), 1963.
[39] M. Cathala, J.-E. Germain, Bulletin of the Chemical Society 6 (1971) 2167–2173.
[40] R. Nilsson, T. Lindblad, A. Andersson, Journal of Catalysis 148 (1994) 501–513.
[41] K.-T. Li, C.-S. Yen, N.-S. Shyu, Applied Catalysis A: General 156 (1997) 117–130.
[42] J.-L. Dubois, WO 2011098706, (Arkema), 2011.
[43] R. Hank, H. Schilling, Makromolekulare Chemie 76 (1964) 134–146.
[44] C.D. Wagner, Faraday Discussions of the Chemical Society 60 (1975) 291.
[45] N. Burriesci, F. Garbassi, M. Petrera, G. Petrini, Journal of the Chemical Society, Faraday Transactions 1 78 (1982) 817.
[46] I. Aso, S. Furukawa, V. Yamazoe, T. Seiyama, Journal of Catalysis 64 (1980) 29–37.
[47] M. Carbucicchio, G. Centi, F. Trifirò, Journal of Catalysis 91 (1985) 85–92.
[48] M.D. Allen, M. Bowker, Catalysis Letters 33 (1995) 269–277.
[49] M. Bowker, C.R. Bicknell, P. Kerwin, Applied Catalysis A: General 136 (1996) 205–229.
[50] A.L. de Abreu, I.R. Guimarães, A.d.S. Anastácio, M.C. Guerreiro, Journal of Molecular Catalysis A: Chemical 356 (2012) 128–136.
[51] E.G. Bithell, R.C. Doole, M.J. Goringe, M.D. Allen, M. Bowker, Physica Status Solidi (a) 146 (1994) 461–475.
[52] E. v. Steen, M. Schnobel, R. Walsh, T. Riedel, Applied Catalysis A: General 165 (1997) 349–356.
[53] H. Zhang, K. Sun, Z. Feng, P. Ying, C. Li, Applied Catalysis A: General 305 (2006) 110–119.